Journal of Instrumentation

PAPER • **OPEN ACCESS**

Review of SIRIO interferometer experimental results

To cite this article: C. Mazzotta 2023 *JINST* **18** C08007

Published by IOP Publishing for Sissa Medialab

Received: *March 1, 2023*
Accepted: *May 1, 2023*
Published: *August 11, 2023*

6TH International Conference Frontiers in Diagnostics Technologies
ENEA Frascati Research Centre, Frascati, Italy
19–21 October 2022

Review of SIRIO interferometer experimental results

C. Mazzotta

ENEA,
via E. Fermi 45, 00044 Frascati RM, Italy

E-mail: cristina.mazzotta@enea.it

Abstract: The SIRIO (Scanning InfraRed Interferometer) interferometer [1], recently disassembled together with the FTU (Frascati Tokamak Upgrade) experiment [2], worked continuously from 2004 to 2019.

An extremely important contribution was made in all the experiments conducted on this tokamak. By virtue of its characteristics, in terms of spatial (1 cm) and temporal resolution (density profiles every 62 μs), combined with its capability to scan the entire plasma column. This interferometer produced all the density feedbacks for operations. Above all, it collected accurate density measurements in plasma physics, among the best data of all tokamak interferometers.

In this review, it is reported the highly valuable experimental work of this powerful diagnostics. Indeed, high density observations were analyzed, as well as fast variations were measured; some examples: the detection of plasma instabilities (MARFE), the trace and the speed of the pellets, the measurement of the particle transport efficiencies in important transients etc.

In order to improve the knowledge for future interferometry in plasma density measurements projects, some topics related to data analysis are also exposed, as well as local density reconstruction methods.

Keywords: Interferometry; Plasma diagnostics - interferometry, spectroscopy and imaging

https://doi.org/10.1088/1748-0221/18/08/C08007

Contents

1 Introduction

Interferometry is currently the most accurate and reliable diagnostic equipment for obtaining electron density measurements in fusion devices, and it is commonly used in all plasma configurations and conditions.

However, the use of shorter wavelength sources to increase resolution has made the vibrations of optical components relevant, contributing significantly to the interferometric phase. The most frequently used in interferometry for plasma density are the IR sources, anyway in some cases, relevant density gradients as well as mechanical vibrations cannot be neglected and a compensation system is required. To address this, many tokamaks employ the so-called Two-Colour Interferometer (TCI) [3–7]. Moreover, the interferometer here described is equipped with a scanning beam (equivalent to a multi-chord system) that provides the maximum spatial resolution.

2 SIRIO peculiarities

In the first years of FTU [2] operations a 5-channel DCN interferometer ($\lambda = 195\,\mu m$) and subsequently, a 2-channel CO2/visible one, were used to collect electron density measurements as well as for density feedback necessary during the operations. However, the need for improved spatial resolution arose as a result of specific experimental campaigns, such as studying the plasma response to pellets. In response, the RFX Consortium [8] designed and installed a scanning interferometer on FTU at the end of 2003. It was one of the first scanning interferometers to be used on a tokamak [1, 9, 10].

In order to compensate the vibrations, produced by optical and mechanical components, in environments polluted by noise, such as a tokamak, a TCI have made necessary. Furthermore, this type of interferometer is useful also to manage relevant density gradients often present in the FTU experiments.

The following subsections will discuss the choice of wavelength for SIRIO in relation to FTU characteristics and plasmas, as well as the "scanning" concept that greatly improves spatial resolution.

2023 JINST 18 C08007

2.1 Choice of the wavelength

In the interferometry, for instance in a in Mach Zender type, the quantity measured is the phase shift Φ, this is proportional to λ. However, vibrations of mechanical structures contribute to the phase shift and are inversely proportional to λ. Therefore, the measured phase shift contains both components.

If L is the chord length, n is the line electron density and δ_{vib} is the total excursion of the optical path due to vibrations, the following approximations, which are valid for relatively short wavelengths, summarize the lengths:

$$\Phi_{\text{pl}} = \frac{\lambda e^2}{4\pi c^2 \varepsilon_0 m_e} \int_L n\,(x)\,dx \tag{2.1}$$

$$\Phi_{\text{vib}} = \frac{2\pi\delta_{\text{vib}}}{\lambda} \tag{2.2}$$

the Δ_Φ results to be of the order of $10^{-15}\ \lambda L N_0$ for FTU typical values: $N_0 = 10^{20}\,\text{m}^{-3}$, $\boldsymbol{L} \ll 1\,\text{m}$, $\delta_{\text{vib}} \gg 100\,\mu\text{m}$. It's clear that longer wavelengths are preferred, in fact the effect of the vibrations decreases and the plasma effect increases. For these densities and abrupt rise of them, e.g. due to pellet injection, the CO2 laser can be considered. In fact, if λ is 10.6 µm 1 fringe is of the order of $10^{20}\,\text{m}^{-3}$, and a few dozen of fringes per second can be obtained, so an acquisition rate of a few kHz is sufficient to collect data.

The previous interferometer used on FTU was a DCN laser (λ = 195 µm), with this wavelength higher variations are reached (of the order of 5×10^4 fringes/s). For this type of lasers the "Veron wheel" [11, 12] is used to realize the heterodyne system, but in this case, the beating frequency became of the same order, in fact, it gives a Doppler shift up to 100 kHz, so the reconstruction of the fringes number would have been impossible.

The wavelength chosen for compensation in SIRIO is that of a CO laser (λ = 5.4 µm), which ensures optimization of the heterodyne system and signal reconstruction during a fringe jump. Finally, it should be noted that since both wavelengths are invisible, the interferometer was equipped with a visible laser to aid in alignment.

2.2 The scanning system

In the figure 1 the scheme of SIRIO interferometer is depicted. The beam paths can be described as follow: starting from the two lasers, as mentioned before, a CO2 laser (10 W, λ = 10.6 µm) for the density measurement and a CO (1 W, λ = 5.4 µm) for compensation, they cross the respective Bragg cells, indicated as BC in the scheme. Indeed, to collect data by a single-photoconductive detector for each chord, two Bragg cells realize different frequency shifts for heterodyne detection, in particular 30 MHz for the CO and 40 MHz for the CO2. In this way, a dichroic mirror can combine the two colors and, at the end, the signals are electronically split for the analysis.

The figure 1 reports the path of the scanning chord, it is thrown vertically from bottom to top, and spatially deflected side to side, in order to sweep the entire plasma cross section, by an oscillating mirror at a high frequency. The integrated electron density is measured along the scanning beam, this one is separated in time by reconstructing a density profile for each half-period of the scan.

Due to an obstruction in the middle of the port, two scanning beams are used to cover the entire aperture of the 400 mm FTU port. In addition to the scanning beams, three fixed chords were also

2023 JINST 18 C08007

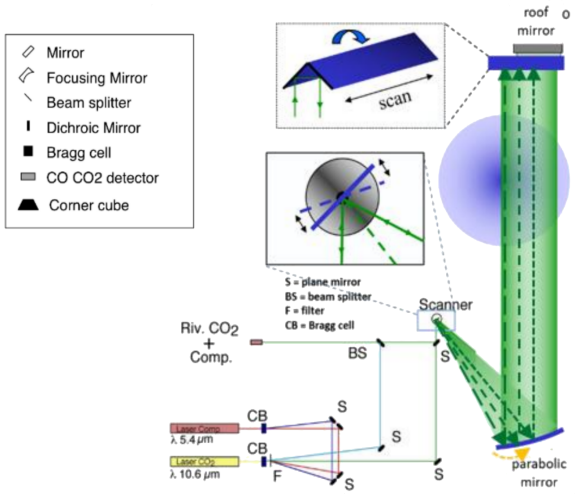

Figure 1. Scheme of SIRIO interferometer, scanning chord path.

realized and used to assess the scanning beam reconstruction. The beams, after crossing the plasma, are reflected by a 'roof-top' retro-reflector made by two rectangular flat mirrors forming a right angle. As this is not a typical corner cube, it is necessary to cancel its deflection by collecting the beam with the same parabolic mirror and reflecting it back. SIRIO is a multi-chord interferometer, in the figure 1 only the path of one scanning chord is depicted, the other ones are not shown for clarity of the figure.

In the central box of the figure 1, the detail zoom of the oscillating mirror is shown. Its dimensions are 6×4 mm and it is placed at the focus of an ad hoc parabolic mirror. This is the most innovative and delicate optical component, it is used to scan the laser beam within the port. In order to build this oscillating mirror some strict specifications for the system are needed: a scanning angle of the order of a few degrees and a scanning frequency higher than 5 kHz. Such a frequency, in conjunction with a sampling frequency of 500 kHz, allows to obtain a complete 40-chord profile in 100 ms. An acousto-optical deflector called CRS (counter-rotating scanner) meets the required specifications, in terms of sweeping angle and frequency. It is an electromagnetic motor where the rotor (to which the mirror is fixed) is oscillated at its electromechanical resonance frequency. By acquiring the CRS signal synchronously with the detected signal of the scanning chord, the splitting into a set of spatially separated chords is reconstructed by software elaboration, also averaging data within the beam diameter. Depending on the ratio between scan amplitude and beam diameter (1 cm) a number of equivalent chords are derived. To obtain better reliability of the CRS, it was decided to work at 8 kHz making a number of strings between 28 to 34 depending on the scan amplitude. A potential disadvantage of the scanning system is the not simultaneity of the measurement for the different elaborated chords. This approximation is acceptable for most of plasma phenomena that typically occur at a time scale much longer than the scanning time.

It should be noted that even in the best alignment, mechanical vibrations due to an incomplete overlap of the two colors are not perfectly compensated. This error is reproducible in time, as the defective cancellation of the deflection, and so it is subtracted using data before the rise of density during a pulse. Being the rooftop mirror stuck directly to FTU port, an effect on the tilt is found, it can have am-

2023 JINST 18 C08007

plitude up to 1 mrad. A correction can be attempted by comparing the computed tilt, before and after the discharge (as a sort of bias), with the computed density. However, in worst cases, a residual systematic error may still be present in the data. Nevertheless, all interferometers employ a large rooftop mirror to obtain high spatial resolution, so this error is not inherent to the scanning interferometer.

Altogether the noise found was approximately $\sim 2 \times 10^{18}\,\mathrm{m}^{-2}$.

3 Review of some experimental results

The FTU characteristics made this experiment particularly suitable to develop advanced scenarios at significant magnetic fields and densities. It is a compact high magnetic field tokamak having a major radius of 0.93 m, a minor radius of 0.3 m, at high toroidal magnetic field (BT up to 8 T) and plasma current (I_p up to 1.6 MA), a metallic chamber operating with a TZM toroidal limiter (99% molybdenum) and a stainless steel AISI 304 vacuum chamber [2]. The next subsections contain some experiments, in which the relevant data collected by the SIRIO interferometer are exhibited.

3.1 High densities in Lithium limiter and pellets

The FTU's unique characteristics have enabled specific studies in the field of edge physics, with important results regarding high density plasmas. Some experimental campaigns were dedicated to the Liquid Lithium Limiter (LLL), beneficial effect on the plasma were assess. Figure 2 shows the raw profiles of discharge #28510 ($I_p = 0.5\,\mathrm{MA}$, $n_e = 0.710^{20}\,\mathrm{m}^{-3}$, $B_t = 6\,\mathrm{T}$) at different times, which was performed by inserting the LLL inside the vacuum vessel [13]. The electron density n_e doubled during the pulse, growing up to $2 \times 10^{20}\,\mathrm{m}^{-3}$ ($\sim n_{GW}$; blue and green points after the doping, red and purple before), twice the pre-programmed value, and remained almost constant for about 0.4 s, despite no gas being fuelled into the vessel. Several publications detail the beneficial effect of this limiter in FTU plasmas [14]. In the figure, the line density data are reported (integral measurements) as profiles at different times. The hole in the profile comes from the port obstruction; indeed the data are collect by using two scanner beams.

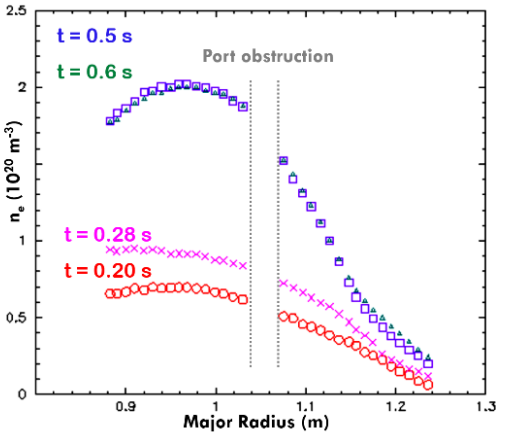

Figure 2. Line densities for #28510 before and after LLL insertion (0.4 s).

3.2 Inverted density profiles

To obtain an accurate density measurements, possible thanks to the high spatial resolution, a reconstruction of inverted density profiles is required, also known as "local density". Two methods for inverting density profiles have been used so far, both are performed assuming the density as function of the poloidal magnetic flux (Φ). For most density profiles, the Cormack technique [15, 16] is used, which involves an expansion in polynomials for profile inversion. However, in some cases, an asymmetric Abel inversion algorithm, which uses the line-integrated data without any fitting,

2023 JINST 18 C08007

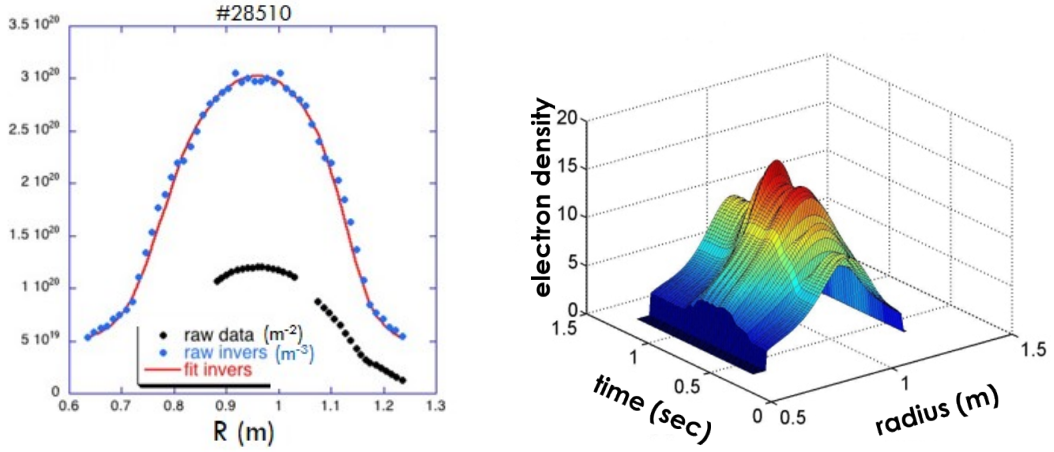

Figure 3. At left the local density: integral (black dots) and inverted profiles (red trace) reconstructed by Cormak method; at right a 3D contour plot.

proves to be more effective. Figure 3 on the left shows the points obtained using the Cormack method of inversion for the same pulse reported in figure 2; that is how the SIRIO interferometer allows getting 3D shape of local density at high spatial and temporal resolution (figure 3 at right).

Having high-resolution data and corresponding inverted density profiles have been found to be very helpful in pellet studies. Indeed, by using of the older 2-channel CO2/visible interferometer, the density increase is visible when the pellets were launched, but it is not possible to reconstruct a profile with only two chords and the effect of a possibly non-symmetrical density rise cannot be deduced, even the ablation and pellet velocity can only be estimated approximately.

In figure 4, a pulse with two pellets injected is illustrated with data collected by SIRIO. On the left, the line density of the chords from the centre (R = 0.95 m) to the edge of the FTU torus (R = 1.2 m) is shown. In the central frame, a 2D contour plot in the time slice around the launch of the second pellet (t = 1.06 s) is shown; in this case, the peripheral entrance of the pellet produces an edge elevation of the density profile. On the right, the 3D contour plot in the same time slice highlights this hollow shape very well [1, 17].

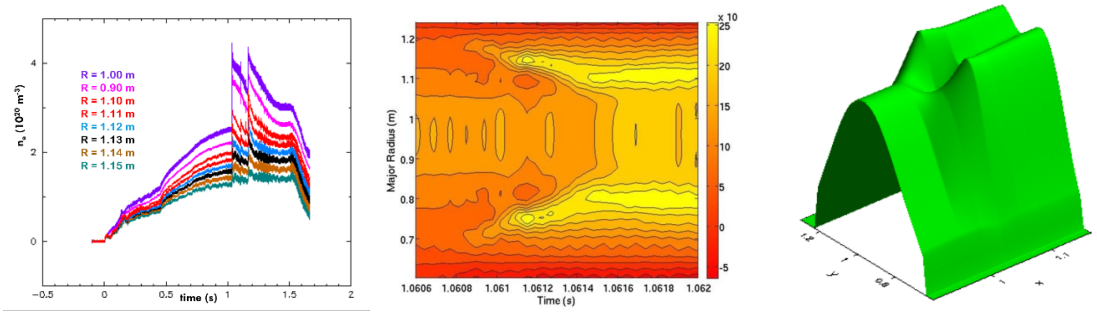

Figure 4. At left: time evolution of the pulse #25255, different colours for different chords. Two pellets are injected, the second one at 1.06 s. The central and right figures are referred to this time. In the centre: the 2D local density and, at right the 3D shape, both show the hallow profile due to the pellet during its ablation.

2023 JINST 18 C08007

3.3 MARFE detection

The MARFE (Multifaceted Asymmetric Radiation From the Edge) is a plasma instability. It is ring of strong radiation, toroidally symmetric and poloidally localized in the high-field side (HFS) of a tokamak chamber, appearing above a density threshold related to the plasma current [18–20]. In FTU the MARFE instability appears when the average electron density is of the order of $\overline{n} \sim 0.5 n_G$ [21], with $n_G = I_p(MA)/\pi a^2$, at the same time the plasma edge temperature drops, the D_α signal increases and the visible light camera shows a toroidal ring of strong emission from this zone (figure 5 at left). Some MARFEs move poloidally, other ones MARFEs evolve into detached plasmas after moving poloidally. Often it is observed as fast oscillations in the line density signal; this last case is the second type of MARFE, as above mentioned [22, 23]. The oscillations are because this part of dense and cold plasma intercepts the chords of the interferometer, as shown in figure 5 on the right upper frame. In the zoom an ovoid (green) has been drawn which represents the MARFE, swinging up and down causes oscillations of the signal (central frame). The profiles (at right below in the figure) are no longer symmetrical, so it is difficult to obtain a reconstruction of the real local density. This is because inversion methods assume a poloidal symmetry of the plasma. However, since the SIRIO interferometer is capable to detect the presence of the MARFE and, thanks to its spatial resolution, determine its position, it has been possible to carry out studies, which confirm the dependence of the MARFE on the drift effect [23, 24] and carry out analysis on oscillation frequencies [23]. In the box at the bottom of the figure, in the upper square, the oscillations on the interferometric signal are clearly visible, in the lower frame the light stripes are the frequencies of the spectrum of the oscillations. On the right, the data collected for a single swing, in particular line density profiles of the peak and of the bottom. The data are strongly asymmetrical, due to the MARFE presence, so it is not trivial to perform an inversion.

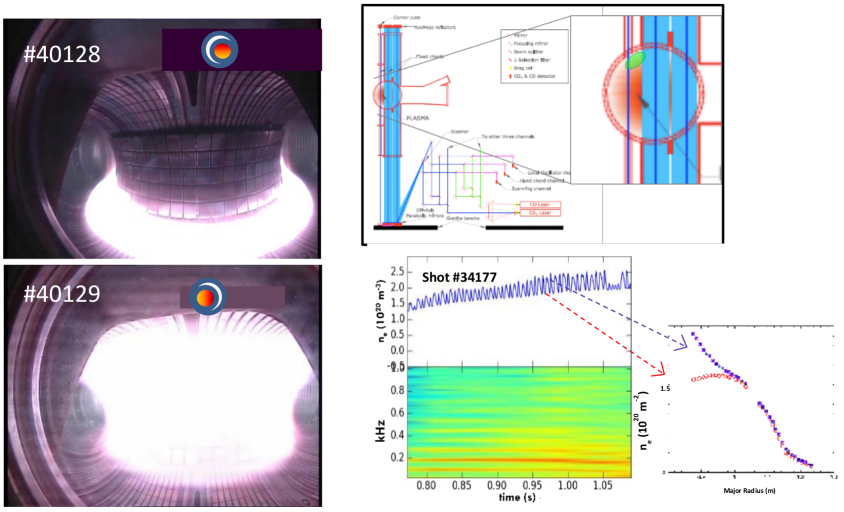

Figure 5. At left: two pictures taken by the visible camera show the MARFE. At right, upper figure, sketch of how the interferometer intercepts the MARFE, an oscillating ovoid (green) contributes to the density of the chord. Lower right box, the oscillating density signal, in the bottom frame the spectrogram. On the right: the respective density profiles of the up and down the oscillation.

2023 JINST 18 C08007

3.4 Particle transport: collisionality, heating and doping effects on density profiles

Regarding the density profiles evolution during the ECRH (Electron Cyclotron Resonant Heating) heating in FTU, only plasmas with ~1 MW of ECRH power and low densities (for FTU of the order of 5×10^{19} m^{-3}) show a clear pump out effect. In such discharges, during the profile evolution, an estimate of the diffusion coefficient and the pinch velocity has been calculated [25, 26], in the plasma core where the neutral source is negligible. For this purpose the particle flux has been written as: $\Gamma/n_e = U - D/n_e \partial n_e/\partial r$, where U is the inward pinch and D the diffusion coefficient. Plotting the flux versus $d(\log n_e)/dr$, for a fixed radius and fitting the data, the two coefficients D and U can be obtained [27]. The calculus of these coefficients, during the first 40 ms of the ECRH phase, are exposed in figure 6.

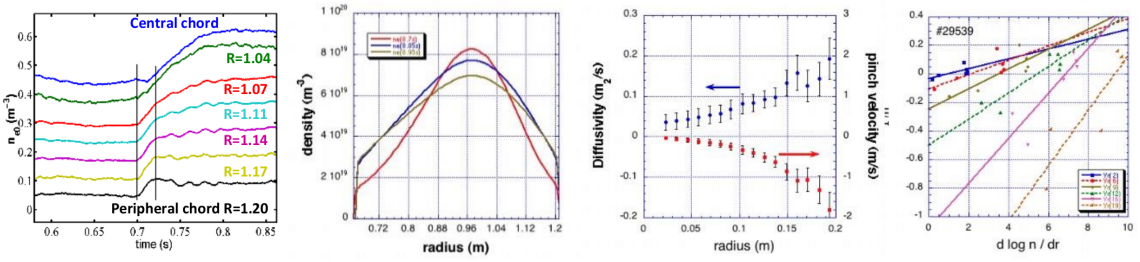

Figure 6. At left, density time traces of a pulse with a presumed pump-out, various colors for different positions. The peripheral chords react immediately at the heating with a stronger increase in respect of central ones. In the 20 msec after ECRH start of the heating the shapes of the profiles flat, subsequently the profile continues to peak (second box, red profile before the ECRH heating phase). Third box: particle pinch velocity. Fourth box: the straight lines found at different radii determine the transport coefficients.

As said, the possibility to reconstruct detailed local density profiles, as well as to obtain well assess peaking factors (defined as $Ne_0/\langle Ne \rangle_{\rm vol}$) has made an important contribution to the numerous studies on high density. Among these, we can mention [28], in which the behavior of Lower Hybrid (LH) heating in the high densities of FTU has been deepened. In particular, some experimental campaigns were devoted to evaluate the LH diffusion of the coupled LH waves power in the plasma and the consequent LHCD (Current Drive), at plasma density even higher than that required on ITER.

Another example of density peaking behavior during LH heating is illustrated in figure 7. The pulse #29222 has additional heating due to Lower Hybrid excitation, that starts around 0.6 s (figure 7.d green trace). The heating is not completely constant during the 400 msec of its duration, so that the temperature profiles (figure 7.a contour plot of the Te profiles) as well as the density profiles, due to kinetic response to the heating, change drastically (frame 7.f contour plot of the high resolution n_e profiles). So, the peaking is affected by this behavior (figure 7.g).

In terms of particle transport, a parameter used to compare the various experiment is the collisionality: $\nu_{\rm eff} = 0.1$ Zeff $\langle n_e \rangle R/\langle T_e \rangle^2$, where $\langle n_e \rangle$ stands for the electron density volume average and $\langle T_e \rangle$ is the electron temperature volume average.

FTU had the opportunity to explore a broad range of collisionality, in particular in the plot peaking factor vs collisionality, its cloud covers the high $\nu_{\rm eff}$ regime for the entire data set, and systematically higher peaking values are reached. It's remarkable that, at high $\nu_{\rm eff}$, the peaking rises proportionally to the $\nu_{\rm eff}$ [29, 30]. At relatively low and medium collisionality, (less than 10

2023 JINST 18 C08007

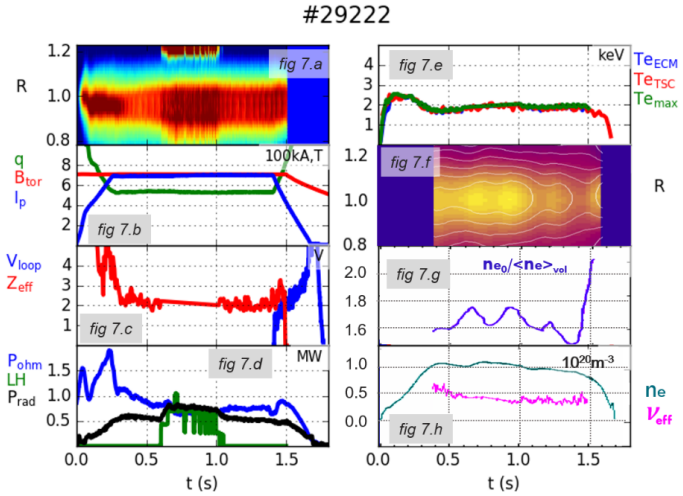

Figure 7. Principal parameters of the pulse #29222 with LH heating.

with $\langle n_e \rangle$ of the order of 10^{19} m^{-3}), the inverse linearity of the density peaking factor versus ν_{eff} is similar to other tokamaks. The FTU data, in this particular range, are exhibit in figure 8, where the colour legend highlights the trend in term of electron temperature, containing the data set pulses with additional heating too [31].

Coming back to the figure 7, the ν_{eff} remains quite unchanged (frame 2.h pink trace) while the peaking is affected by the LH heating.

Finally, we cannot fail to mention the numerous studies on plasmas injected with impurities [32–35], because it is crucial to determine the conditions that favor a strong increase of particle confinement while minimizing the amount of impurities needed, as well as to favor the so-called "plasma detachment". An increase of the electron density with a remarkable values of the peaking factor are reached in FTU doped pulses. The injection consequences are depending not only by the amount of impurity seeding, but also to the rate of injection and plasma condition, in terms of plasma parameters and edge conditioning. The figure 9 exposes the profiles of pulses affected by different doping, at left the density profiles of the shots. The red and pink profiles are referred to pulses where Helium injection was adopted, the dark violet trace is the pulse without impurity, the pulse with Neon injection is colored cyan. In particular, these two latter pulses were produced in the same experimental session (I_p = 360 kA, B_T = 5.2 T): one with a Neon injection at 0.6 s for 50 msec and a second one at the same current and toroidal field, but with exclusively Deuterium gas, reaching the same line-average electron density, to be used as reference undoped pulse. As a consequence of the injection, the doped pulse get colder in the outer region up to half radius. An impressive density peaking rise of Neon injected discharge in respect to the undoped one was found (profiles at left of figure 9), finally also the energy confinement in the central region was found improved. In order to complete experimental observations regarding the electron density peaking in Neon doped plasmas, Helium injection has been realized and achieved even better performance. A search for the best obtainable conditions has made it possible to reach a very high density peaking factor, up to a value of five.

2023 JINST 18 C08007

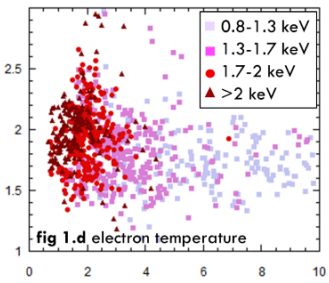

Figure 8. Peaking vs collisionality for a set of FTU low collisionality pulses. The "hot" discharges are in the low ν_{eff} area, the pulses with $T_e < 1.7$ keV drifts towards the high collisionality.

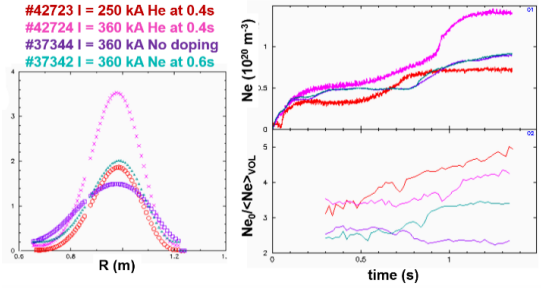

Figure 9. At left, inverted density profiles for doped pulses, they are taken at 1.1 s when the effect of the injection are well assess. In the list of the pulses the time of the injection is reported. At right, upper frame: line central density, bottom frame: the peaking.

4 Conclusion

The scanning technique overcome the limitations of traditional interferometry thanks to the high number of equivalent measurements channels. From 2004 to 2019, in addition to reliably providing density feedback for all FTU operations, the SIRIO interferometer has made a great contribution in the experiments performed.

In this paper an overview of the capability of the SIRIO interferometer was presented, within the scope of results of the Frascati Tokamak Upgrade (FTU) experiment, which has contributed significantly to the understanding of plasma behavior and transport in tokamaks. The experiments carried out on FTU have provided important insights into various aspects of plasma physics, including particle transport and collisionality studies, better confinement, heating and doping effects on density profiles.

The measurements of peaking factors and diffusion coefficients during Electron Cyclotron and Lower Hybrid heating have helped to describe the mechanisms related to plasma heating and particle transport. Overall, the research conducted on FTU has significantly advanced our understanding of plasma physics and contributed to the development of fusion energy. Furthermore, thanks to the SIRIO data produced, research streams such as pellets injection, MARFE detection were able to explore. The high capability of this diagnostic to get fine reconstruction of density profiles together with its reliability should be considered for future plasma interferometers.

Acknowledgments

The author acknowledges all individuals involved in FTU, listed in all *FTU collaborations* from 2004 to 2020 (the latter in the appendix of G. Pucella et al. Proceedings of the 28th IAEA Fusion Energy Conference, Nice, France, 2021), in particular the ENEA colleagues: O. Tudisco, G. Pucella, E. Giovannozzi, G. Rocchi, also P. Innocente of the RFX Consortium.

2023 JINST 18 C08007

References

[1] C. Mazzotta et al., *Measurement of density profiles using the new infrared scanning interferometer for FTU*, *Phys. Scr.* **T123** (2006) 79.

[2] C. Gormezano et al., *Chapter 1: The FTU program*, *Fusion Sci. Technol.* **45** (2004) 297.

[3] T. Luke and J.H. Irby, *Density Measurements on Alcator C-mod*, *Bull. Am. Phys. Soc.* **38** (1993) 1955.

[4] T.N. Carlstrom, D.R. Ahlgren and J. Crosbie, *Real-time, vibration-compensated CO_2 interferometer operation on the DIII-d tokamak*, *Rev. Sci. Instrum.* **59** (1988) 1063.

[5] P. Innocente and S. Martini, *A two color multichord infrared interferometer for RFX*, *Rev. Sci. Instrum.* **63** (1992) 4996.

[6] J.H. Irby, E.S. Marmar, E. Sevillano and S.M. Wolfe, *Two-color interferometer system for alcator c-MOD*, *Rev. Sci. Instrum.* **59** (1988) 1568.

[7] M.A.V. Zeeland et al., *Tests of a two-color interferometer and polarimeter for ITER density measurements*, *Plasma Phys. Control. Fusion* **59** (2017) 125005.

[8] A. Canton et al., *Spatially scanned two-color mid-infrared interferometer for FTU*, *Rev. Sci. Instrum.* **72** (2001) 1085.

[9] O. Tudisco et al., *Chapter 8: The diagnostic systems in the FTU*, *Fusion Sci. Technol.* **45** (2004) 402.

[10] P. Innocente, A. Canton, C. Mazzotta and O. Tudisco, *Scanning beam medium infra-red interferometry for plasma density measurements*, *J. Phys. Conf. Ser.* **227** (2010) 012006.

[11] D. Veron, *Interferometry in large plasma machines, in Diagnostic for Fusion Reactor Conditions*, Proc. Workshop, Varenna (1982), CEC, Brussels (1982), Vol. 1, p. 199–223.

[12] D. Veron, *Submillimeter Interferometry of High-Density Plasmas*, in *Infrared and Submillimeter Waves*, K.J. Button ed., Academic Press, New York (1979), Vol. 2, p. 69.

[13] G. Mazzitelli et al., *Lithium as a Liquid Limiter in FTU*, in *Proceeding at 21st IAEA Fusion Energy Conference*, Chengdu, China, 16–21 October 2006.

[14] G. Mazzitelli et al., *Review of FTU results with the liquid lithium limiter*, *Fusion Eng. Des.* **85** (2010) 896.

[15] A.M. Cormack, *Representation of a function by its line integrals, with some radiological applications*, *J. Appl. Phys.* **34** (1963) 2722.

[16] A.M. Cormack, *Representation of a function by its line integrals, with some radiological applications. II*, *J. Appl. Phys.* **35** (1964) 2908.

[17] E. Giovannozzi et al., *Vertical pellet injection in FTU discharges*, *Nucl. Fusion* **45** (2005) 399.

[18] B. Lipschultz, *Review of MARFE phenomena in tokamaks*, *J. Nucl. Mater.* **145-147** (1987) 15.

[19] F.P. Boody et al., *Phenomenology of MARFEs in TFTR*, *J. Nucl. Mater.* **145-147** (1987) 196.

[20] M.Z. Tokar, *Non-linear effects in particle and heat balances of edge plasmas*, *Contrib. Plasma Phys.* **32** (1992) 341.

[21] G. Pucella et al., *Density limit experiments on FTU*, *Nucl. Fusion* **53** (2013) 083002.

[22] O. Tudisco et al., *Peaked density profiles and MHD activity on FTU in lithium dominated discharges*, *Fusion Eng. Des.* **85** (2010) 902.

2023 JINST 18 C08007

[23] C. Mazzotta et al., *Dynamic and frequency behaviour of the MARFE instability on FTU*, Nucl. Mater. Energy **12** (2017) 808.

[24] A.V. Chankin, *On the poloidal localization and stability of multi-faceted asymmetric radiation from the edge (MARFE)*, Phys. Plasmas **11** (2004) 1484.

[25] V. Zanza et al., *Particle transport in the Frascati Tokamak upgrade*, Nucl. Fusion **36** (1996) 825.

[26] O. Tudisco et al., *Density profile studies of plasma with Lithium Limiter*, in *2006* 33^{rd} *EPS Conf. on Plasma Phys.*, Rome, Italy (2006), ECA Vol. 30I, P-1.073.

[27] C. Mazzotta et al., *Particle density behaviour in FTU electron heated plasmas*, in *2008* 35^{rd} *EPS Conf. on Plasma Phys.*, Hersonissos (2008), ECA Vol. 32D, P-2.026.

[28] R. Cesario et al., *Current drive at plasma densities required for thermonuclear reactors*, Nature Commun. **55** (2010) 1.

[29] M. Romanelli et al., *Parametric dependence of turbulent particle transport in high density electron heated FTU plasmas*, Plasma Phys. Control. Fusion **49** (2007) 935.

[30] C. Mazzotta et al., *Highly collisional regimes in FTU*, in *Proc. of the* 44^{th} *EPS Conf. on Plasma Physics*, Belfast, Northern Ireland, U.K. (2017).

[31] C. Mazzotta et al., *Density profiles in low collisionality FTU plasmas*, in *2019 Proc. of* 46^{th} *EPS Conf. on Plasma Physics*, Milan, Italy (2019).

[32] C. Mazzotta et al., *Peaked density profiles in neon and lithium doped discharges on FTU*, Fusion Eng. Des. **89** (2014) 2853.

[33] C. Mazzotta et al., *Peaked density profiles due to neon injection on FTU*, Nucl. Fusion **55** (2015) 073027.

[34] C. Sozzi et al., *Experiments on magneto-hydrodynamics instabilities with ECH/ECCD in FTU using a minimal real-time control system*, Nucl. Fusion **55** (2015) 083010.

[35] C. Mazzotta, G. Pucella, E. Giovannozzi, M. Marinucci and the FTU Team, *Helium injection plasmas in FTU*, Nucl. Fusion **62** (2022) 026004.

2023 JINST 18 C08007